

Probing the role of highly conserved residues in triosephosphate isomerase – analysis of site specific mutants at positions 64 and 75 in the *Plasmodial* enzyme

Debarati Bandyopadhyay¹, Mathur R. N. Murthy¹, Hemalatha Balaram² and Padmanabhan Balaram¹

¹ Molecular Biophysics Unit, Indian Institute of Science, Bangalore, India

² Molecular Biology and Genetics Unit, Jawaharlal Nehru Centre for Advanced Scientific Research, Bangalore, India

Keywords

amino acid conservation; conserved residues in enzymes; enzyme structure and function; mutational effects on triosephosphate isomerase; triosephosphate isomerase

Correspondence

P. Balaram, Molecular Biophysics Unit, Indian Institute of Science, Bangalore 560012, India
Fax: +9180 2360 0535
Tel: +9180 2293 3000
E-mail: pb@mbu.iisc.ernet.in

(Received 12 June 2015, revised 8 July 2015, accepted 16 July 2015)

doi:10.1111/febs.13384

Highly conserved residues in enzymes are often found to be clustered close to active sites, suggesting that functional constraints dictate the nature of amino acid residues accommodated at these sites. Using the *Plasmodium falciparum* triosephosphate isomerase (*PfTIM*) enzyme ([EC 5.3.1.1](#)) as a template, we have examined the effects of mutations at positions 64 and 75, which are not directly involved in the proton transfer cycle. Thr (T) occurring at position 75 is completely conserved, whereas only Gln (Q) and Glu (E) are accommodated at position 64. Biophysical and kinetic data are reported for four T75 (T75S/V/C/N) and two Q64 (Q64N/E) mutants. The dimeric structure is weakened in the Q64E and Q64N mutants, whereas dimer integrity is unimpaired in all four T75 mutants. Measurement of the concentration dependence of enzyme activity permits an estimate of K_d values for dimer dissociation (Q64N = 73.7 ± 9.2 nM and Q64E = 44.6 ± 8.4 nM). The T75S/V/C mutants have activities comparable to the wild-type enzyme, whereas a fourfold drop is observed for T75N. All four T75 mutants show a dramatic fall in activity between 35 °C and 45 °C. Crystal structure determination of the T75S/V/N mutants provides insights into the variations in local interactions, with the T75N mutant showing the largest changes. Hydrogen-bond interactions determine dimer stability restricting the choice of residues at position 64 to Gln (Q) and Glu (E). At position 75, the overwhelming preference for Thr (T) may be dictated by the imperative of maintaining temperature stability of enzyme activity.

Database

Structural data have been deposited in the Protein Data Bank under accession numbers [4ZZ9](#), [5BMW](#), [5BMX](#), [5BNK](#) and [5BRB](#).

Introduction

Protein sequences bear the imprint of the selective pressures of evolution. Examination of sequences of enzymes, derived from a large set of diverse organisms,

reveals that relatively few residues are completely conserved across all species. Fully conserved residues are likely to be critically important for maintaining opti-

Abbreviations

ANS, 1-anilino-8-naphthalene sulfonate; DHAP, dihydroxyacetone phosphate; GAP, glyceraldehyde-3-phosphate; LC, liquid chromatography; *Lm*, *Leishmania mexicana*; PDB, Protein Data Bank; *Pf*, *Plasmodium falciparum*; TIM, triosephosphate isomerase; TWT, *PfTIM* wild-type.

mal catalytic activity, either by contributing directly to the chemistry of catalysis or, more indirectly, by being indispensable for folding, stability and oligomerization of enzymes [1]. Sequence comparisons over large datasets can also reveal specific sites at which minimal amino acid replacements are observed, suggesting that functional selection imposes severe constraints on the nature of the amino acid side chains that can be accommodated at these positions [2]. The role of consensus mutations at significantly conserved position on protein thermal stability has been explored in an extensive study of *Saccharomyces cerevisiae* triosephosphate isomerase (EC 5.3.1.1) [3,4]. Using the malarial parasite *Plasmodium falciparum* (*Pf*) triosephosphate isomerase (TIM) as a model system, we have been exploring the role of highly conserved residues on structure and function [5,6]. TIM is arguably one of the best studied enzymes in the literature of biochemistry [7–12], earning the distinction of being labelled as the ‘perfect enzyme’ [13]. Its central role in glycolysis ensures that it is ubiquitous in nature. Recent studies also highlight the nonglycolytic roles of glycolytic enzymes, including TIM [14,15]. The growing database of protein sequences derived from genomic data has been used to generate a dataset of 3398 TIM sequences from bacterial sources [16]. Ten residues (K12, T75, H95, E97, C126, E165, P166, G209, G210 and G228) are fully conserved (the numbering scheme used corresponds to the sequences of the yeast and *Pf* enzymes). Of these, the roles of K12, H95 and E165 have been extensively explored in the seminal work of Knowles and coworkers [17–24], which laid the foundation for the current understanding of the mechanistic details of the isomerization reaction [25]. In previous work, we have explored the role of C126 and E97, using specific mutational replacements. Although the former appears to indirectly determine the stability of dimeric enzyme [5], a direct role in the catalytic proton transfer cycle has been suggested for the latter [6].

In the present study, we address the role of the fully conserved T75 residue, which is involved in key hydrogen-bond interactions across the dimer interface. We also examine the consequences of residue replacement at position 64, a site at which Q is present in 3011 sequences, whereas E is present in 383 sequences, in the dataset examined. Q64 is involved in hydrogen-bond interactions across the dimer interface and in intra-subunit interactions with residues proximal to the active site K12 residue. Interestingly, a study by Williams *et al.* [26] on the E65Q mutant of the enzyme from *Leishmania mexicana* (*Lm*TIM; E65 in *Lm*TIM is structurally equivalent to Q64 in *Pf*TIM) reveals a large increase in thermal stability.

The integrity of the enzyme active site, which lies close to the dimer interface, is determined by inter-subunit interactions, making TIM an obligatory dimer. Attempts to engineer monomeric TIMs yielded well folded $\beta_8\alpha_8$ TIM barrels with highly impaired activity, with the catalytic rates dropping by three orders of magnitude [27]. In the present study, we assess the effects of mutations at residues 75 and 64 on TIM dimers using the *Pf* enzyme as a template.

Results

In the present study, four mutants at position 75 (T75S/T75V/T75C and T75N) and two mutants at position 64 (Q64E and Q64N) were examined. Figure 1 shows the interactions involving the side chains of Thr75 and Gln64. The side-chain -OH group of Thr75 makes two important inter-subunit contacts with the Asn10 -NH₂ and Glu97 carboxyl group, whereas the backbone -NH and backbone -CO are connected to the Glu97 carboxyl and Arg98 guanidinium group, respectively. The Gln64 side-chain -CO forms an inter-subunit hydrogen bond to the Gly76 backbone -NH, while the side-chain -NH₂ group forms two hydrogen bonds with the backbone -CO groups of Lys12 and Phe42. Inspections of these interactions suggest that mutations at these sites might perturb dimer interface stability and may also influence activity, in view of the proximity of these residues to the active site residues Lys12, His95 and Glu97 [5]. All mutant proteins were characterized by ESI-MS (data not shown) and their corresponding DNA sequences were determined, to establish their identity.

Biophysical studies

Figure 2 shows the gel filtration profiles for both the sets of mutant proteins. All four Thr75 mutants elute at the same position as that of the wild-type enzyme, confirming that stable dimers are formed under the conditions used. In contrast, both Q64E and Q64N mutants elute more slowly from the column, suggesting that dimer dissociation and equilibration on the column do occur in these cases. CD spectra of the four Thr75 mutants showed that both near and far UV-CD bands were very similar to those observed for the wild-type protein (TWT) (data not shown). Figure 3 compares the spectra for both the wild-type and T75V mutant. In contrast, the Q64E and Q64N mutants possess distinctively different spectral characteristics. In both cases, there is almost complete abolition of the near UV-CD band, centered at approximately 280 nm. Although it is not possible to unambiguously ascribe this band to con-

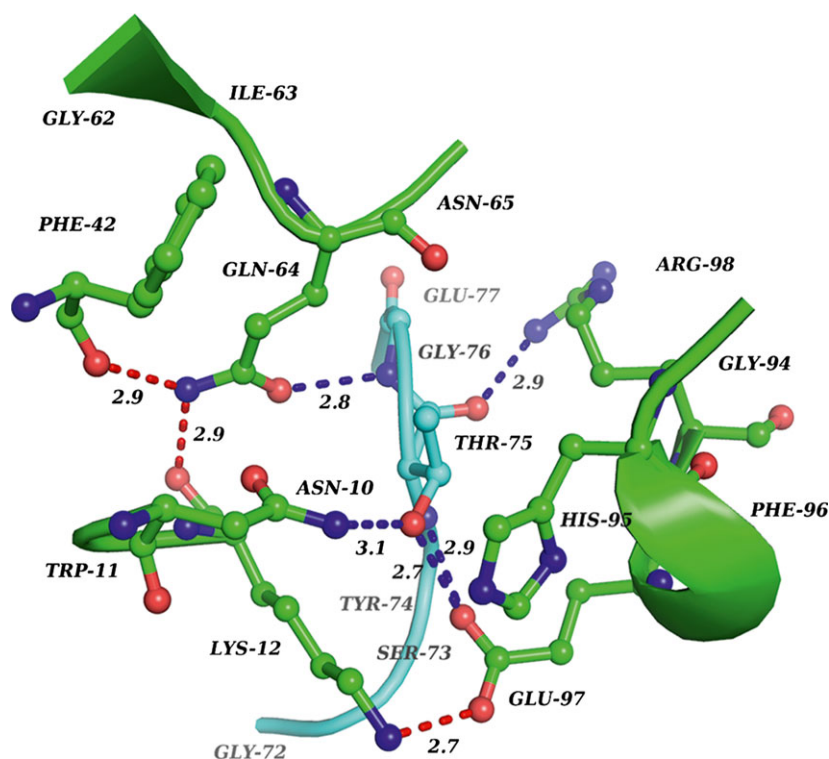


Fig. 1. Environment of Gln64 and Thr75 in *PFTIM* (PDB code: [1O5X](#)). The important network of hydrogen bonds in the dimer interface; Gly72 to Glu77 (in cyan) is from the other subunit. Inter-subunit hydrogen-bonding interactions are shown in blue and intra-subunit hydrogen-bonding interactions are shown in red.

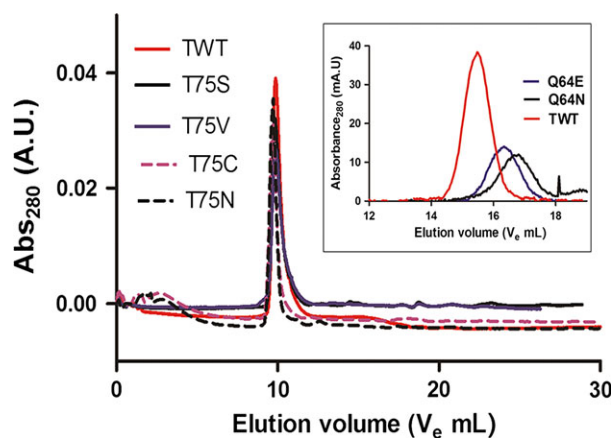


Fig. 2. Elution profiles for all six mutants (T75S/V/C/N; Q64N/E) in inset) and *PFTIM* wild-type (TWT). The protein concentration was 20 μM .

tributions from a specific aromatic residue, it may be noted that Trp (W) 11 is very close to the site of mutation. Interestingly, the aromatic CD band is also lost in the case of the wild-type protein at pH 3, a feature noted in earlier studies [28]. The spectral differences between TWT and Q64E/N mutants are less pronounced in the far UV region, although there is a distinct reduction in the ellipticities at 220 nm. This region contains contributions from both backbone amide and side-chain aromatic group electronic transitions. The

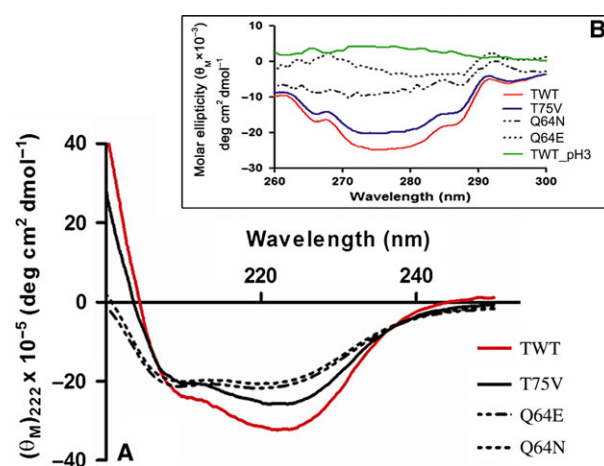


Fig. 3. CD spectra of TWT and the three mutants (Q64N/E; T75V). (A) Far UV-CD (protein concentration: 5 μM) and (B) near UV-CD (inset; protein concentration 30 μM).

Q64E and Q64N mutants also show significant binding of the hydrophobic fluorescent probe 1-anilino-8-naphthalene sulfonate (ANS) at neutral pH (Fig. 4). The wild-type enzyme and the Thr75 mutants do not cause an enhancement of ANS fluorescence intensity. ANS binding and loss of tertiary CD bands as a result of aromatic residues have been correlated in literature to molten globule state of proteins [29,30]. TIM has been shown to bind ANS at low pH values of approximately

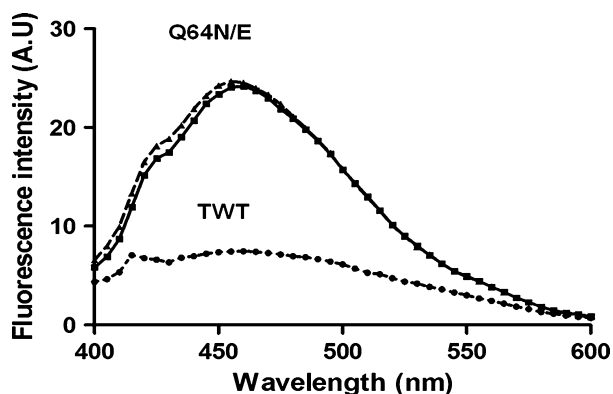


Fig. 4. Fluorescence emission spectra of bound ANS to TWT and the Q64N/E mutants. The protein concentration was $5 \mu\text{M}$ and the ANS concentration was $2 \mu\text{M}$ ($\lambda_{\text{excitation}} = 370 \text{ nm}$).

3, where an acid expanded state of the protein is obtained [28]. The magnitude of the enhancement at acidic pH is significantly more than that shown in Fig. 4 (data not shown). The limited enhancement observed in the case of Gln (Q) 64 mutants may be a consequence of ANS binding at a relatively polar site at the dimer interface, which becomes accessible upon perturbation of inter-subunit interactions. Further evidence of ANS binding to the Q64E/N mutants is also obtained by excitation of the intrinsic fluorescence of the protein at 280 nm. Although no Trp-ANS energy transfer is observed in the case of the wild-type protein, significant transfer is observed for both mutants (data not shown). When ANS binding is monitored as a func-

tion of pH, a dramatic enhancement between pH 3 and 4 is observed for the wild-type protein. A significantly greater enhancement was observed for both mutants between pH 4 and 4.5, suggesting that mutations at this site destabilize the protein with respect to acid-induced unfolding.

*Pf*TIM undergoes irreversible thermal unfolding and aggregation resulting in precipitation of the protein at temperatures $> 50 \text{ }^\circ\text{C}$. The four T75 mutants and Q64E behave like the wild-type enzyme in precipitating at temperatures $> 50 \text{ }^\circ\text{C}$. The Q64N mutant exhibits a thermal precipitation temperature that is significantly lower, at approximately $42 \text{ }^\circ\text{C}$. The thermal unfolding and precipitation of these proteins are preceded by a structural transition in the pre-melting region, which results in distinct changes in CD spectra at temperatures below the onset of precipitation. As noted earlier, far UV-CD spectra of the wild-type protein and the four Thr75 mutants are largely similar at ambient temperature ($23 \text{ }^\circ\text{C}$). Small changes have been noted in the case of Q64E and N mutants (Fig. 3A). Figure 5 compares CD spectra for wild-type protein and the mutants at position 64 and 75 at temperatures, in the temperature range $40\text{--}45 \text{ }^\circ\text{C}$. In the case of T75N, a blue shift of the long wavelength band (219 nm) is observable, while the spectra for the wild-type and T75C mutant are largely indistinguishable at $40 \text{ }^\circ\text{C}$ (Fig. 5A). T75S and T75V mutants behave in a manner similar to T75C and T75N, respectively. Upon increasing the temperature to $45 \text{ }^\circ\text{C}$, differences are clearly observable for all the T75 mutants as compared

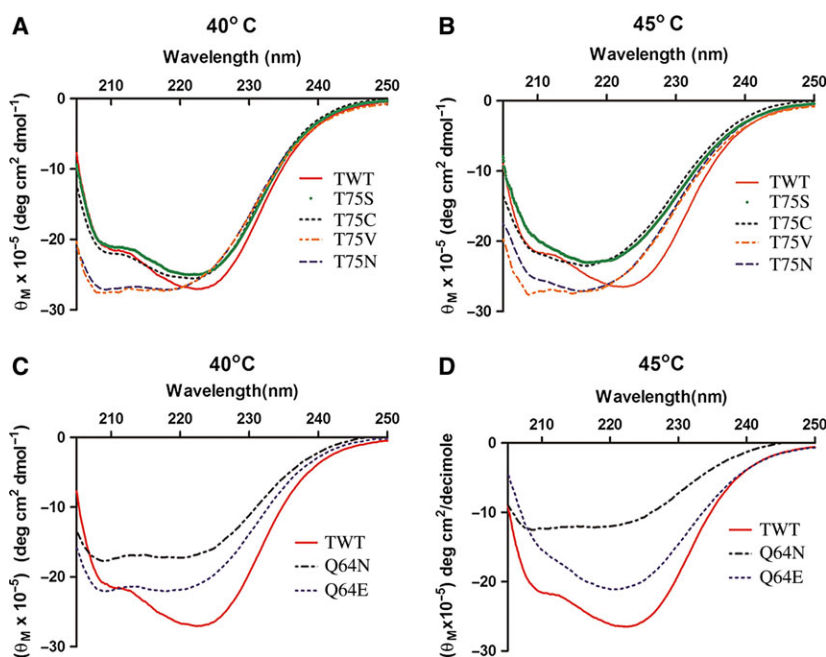


Fig. 5. Thermal melting effect on the mutants. (A, B) On T75 mutants and (C, D) on Q64 mutants at 40 and $45 \text{ }^\circ\text{C}$. The protein concentrations used were $15 \mu\text{M}$. Pathlength = 1 mm .

to the wild-type enzyme (Fig. 5B). Figure 5C,D shows a comparison of the CD spectra of TWT, Q64E and Q64N. At 40 °C, a dramatic reduction of ellipticity in the far UV-CD spectrum of Q64N is observed and even more substantial loss of CD bands is noticeable at 45 °C. The onset of precipitation in the case of Q64N is at a temperature almost 10 °C lower than wild-type protein. In the case of Q64E, small but significant changes are observed at 40 °C, whereas, at 45 °C, there is a distinct change in the band shape presumably corresponding to a pre-melting structural transition. Mutations at positions 64 and 75 destabilize the three-dimensional structure of the enzyme with respect to thermal perturbation. The Q64N mutation appears to be the least thermally stable. The $\beta_8\alpha_8$ barrel fold in TIM has been previously shown to be robust in the presence of high concentrations of urea up to approximately 6 M [31]. All six mutants examined in the present study, unfold in the presence of urea with a midpoint of the structural transition at approximately 3.5–4 M (Fig. 6A) as monitored by shift of the fluorescence emission maxima from approximately 330 nm (folded) to 348 nm (unfolded) and loss of CD ellipticity at 222 nm (Fig. 6B).

The biophysical evidence presented thus far suggests that mutations at positions 64 and 75 destabilize the protein when exposed to thermal perturbation or denaturing agents, such as urea, at ambient temperatures and near neutral pH. The four Thr75 mutants behave in a manner similar to the wild-type enzyme, as indicated by gel filtration studies and spectroscopic properties. Destabilization of subunit interactions appears to result in the case of mutants at position 64.

Enzyme kinetics

Measurements of enzyme activity were carried out over a wide range of protein (0.15–150 nM) and substrate (0.25–4.0 mM) concentrations. Saturation of the measured specific activity was achieved at substrate concentrations > 3 mM for the wild-type enzyme and four Thr75 mutants (data not shown), permitting k_{cat} and K_{m} values to be derived (Table 1). By contrast, saturation of the measured specific activity could not be achieved for the Q64E and Q64N mutants even at D-glyceraldehyde-3-phosphate (D-GAP) concentrations > 4 mM. The Gln64 mutants also had significantly lower activities, necessitating the use of higher enzyme concentrations in the assays (data not shown). Table 1 summarizes the measured activity and kinetic parameters for the wild-type protein, Thr75 mutants and Gln64 mutants. The T75S/V/C mutants were substantially active and exhibited only marginal decreases in

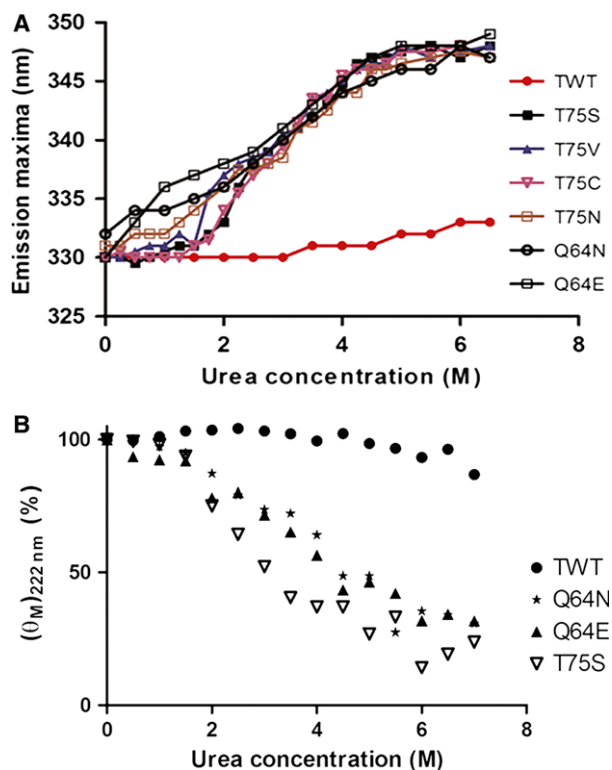


Fig. 6. Urea denaturation study with Q64N/E and T75 mutants at pH 8. (A) Monitoring fluorescence emission maxima and (B) monitoring changes in ellipticity at 222 nm. Protein (5 μM) was incubated with different concentrations of urea for 45 min. The data monitored by CD spectra (B) were normalized by taking the ellipticity at 222 nm in the absence of urea as 100%.

specific activity with respect to the wild-type enzyme. The T75N mutant shows a fourfold reduction in activity. The Q64E and Q64N mutants were significantly less active even at high enzyme concentrations (150 nM), suggesting that both dimer destabilization and conformational alteration at the active site may contribute to the observed five- to 10-fold decrease in specific activity. Figure 7 compares the concentration dependence of specific activity for the Thr75 and Gln64 mutants. Although no dependence of concentration is observed for the wild-type and Thr75 mutants even in the range 0.1–5 nM, a relatively sharp dependence is observed for Q64E and Q64N mutants in the range 5–150 nM. These results suggest that the TIM dimer is unaffected by the mutations at position 75, whereas mutational changes at position 64 led to a considerable loss of dimer integrity.

Making the assumption that the monomeric species is inactive and the measured activity may be ascribed entirely to dimeric species, an estimate of the dimer dissociation constant (K_{d}) for Gln64 mutants may be made, as previously reported by Pray *et al.* [32] for a

Table 1. Kinetic parameters for TWT and all six mutants.

Enzyme	$k_{\text{cat}} \times (10^2 \text{ s}^{-1})$	$K_{\text{m}} \text{ (mM)}$	$k_{\text{cat}}/K_{\text{m}} \times (10^2 \text{ s}^{-1} \cdot \text{mM}^{-1})$	Specific activity ($\mu\text{mol} \cdot \text{mg}^{-1} \cdot \text{min}^{-1}$) [enzyme concentration] ^a
TWT	4.0 ± 0.1	0.62 ± 0.07	6.45	679.6 [5 nM]
T75S	3.8 ± 0.1	0.80 ± 0.08	4.75	573.3 [5 nM]
T75V	3.8 ± 0.2	0.91 ± 0.12	4.18	560.7 [5 nM]
T75C	3.4 ± 0.2	1.15 ± 0.15	2.96	502.4 [5 nM]
T75N	1.3 ± 0.1	0.86 ± 0.08	1.51	178.7 [5 nM]
Q64N ^b	–	–	–	134.1 (301.4) [150 nM]
Q64E ^b	–	–	–	63.3 (126.2) [150 nM]

^a Substrate concentration was 3 mM; assays performed at 23 °C at pH 7.6. Limiting specific activity values for Q64 mutants are given in parenthesis. ^b k_{cat} and K_{m} values could not be obtained since saturation of specific activity could not be achieved at a substrate concentration as high as 4 mM.

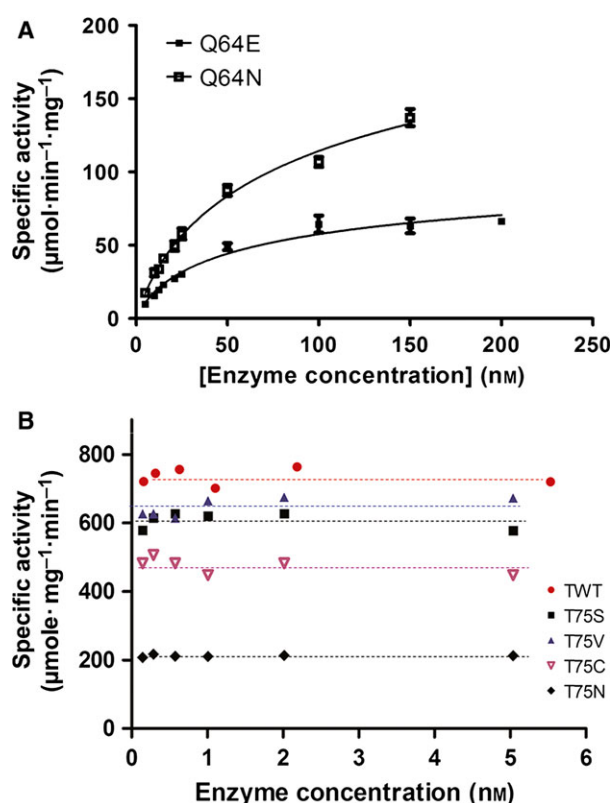


Fig. 7. Dependence of specific activity on enzyme concentrations. (A) For Q64 mutants and (B) for wild-type (TWT) and T75 mutants. All assays were performed at pH 7.6; enzymes at different concentrations were preincubated for 45 min in assay buffer prior to initiation of the assay with 3 mM substrate (D-GAP).

viral protease. The K_{d} values thus obtained are 73.7 ± 9.2 nM for Q64N and 44.6 ± 8.4 nM for Q64E mutants. These values are several orders higher than the estimated value (0.01–0.0001 nM) for the wild-type TIM [33,34]. The assumption of inactive monomers is supported by Borchert *et al.* [27] reporting that engi-

neered monomeric TIM exhibits a 1000-fold drop in measured activity.

To separate the effects of mutations on the local structure of the active site from the effects on dimer stability, it is necessary to estimate the limiting specific activity for the Gln64 mutants. This is readily achieved by fitting the experimental data to the following equations [32] using PRISM, version 5 (GraphPad Software Inc., San Diego, CA, USA) (Fig. 7A).

$$A_{\text{spec}} = A_{\text{max}} \frac{[Pr_2]}{[Pr] + [Pr_2]}$$

$$2 \frac{[Pr]^2}{K_{\text{d}}} + [Pr] - E_{\text{tot}} = 0$$

where A_{max} is the maximum specific activity, A_{spec} is the measured specific activity in the assay, and $[Pr]$ and $[Pr_2]$ are the concentration of free monomer and dimer in the solution. E_{tot} represents the total enzyme concentration used in each assay ($[Pr] + 2[Pr_2]$); $[Pr]$ was derived in terms of K_{d} by using the second equation and eventually A_{max} and K_{d} were solved from the first equation. These yield limiting values of $126.2 \mu\text{mol} \cdot \text{mg}^{-1} \cdot \text{min}^{-1}$ and $301.4 \mu\text{mol} \cdot \text{mg}^{-1} \cdot \text{min}^{-1}$ for Q64E and Q64N mutants, respectively. Thus, an approximately 2.5-fold drop in activity is observed for the Q64N mutant, whereas a significant greater drop of fivefold was observed for the Q64E mutant.

Q64 mutants: pH effects

The replacement of Q at position 64 by E raises the possibility that the ionization state of the glutamic acid side-chain influences the structure of the active site. In the unionized form, the E (Glu) side chain might be expected to minimally perturb the local network of hydrogen bonds, whereas ionization to the carboxylate

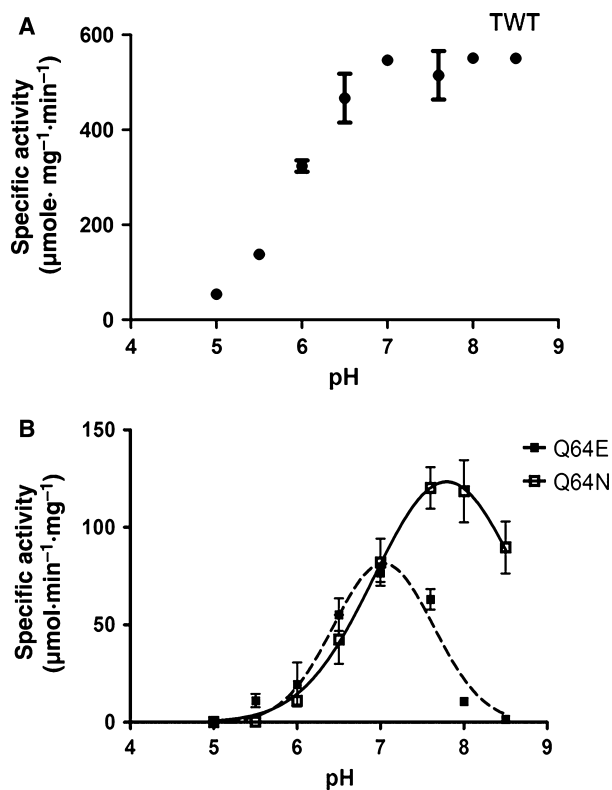


Fig. 8. Specific activities of (A) TWT and (B) Q64N/E mutants at different pH values; 5 nM TWT, 150 nM Q64 mutants and 2 mM substrate (D-GAP) were used in the assay.

may be expected to have appreciable effects on the local structure. Figure 8 compares the pH dependence of the specific activity of the Q64E/N mutants. At pH values below 7, both mutants have comparable activities. The Q64E mutant shows a sharp fall in activity between pH 7 and pH 8, presumably due to titration of the E64 carboxylic acid group. The observed high pK_a of approximately 7.5 may be a consequence of the stabilizing effect of the hydrogen-bonded network on the protonated form of glutamic acid (E) at position 64.

Structural analysis of Q64 mutants

Obtaining crystals diffracting to high resolution ($< 3.0 \text{ \AA}$) for the Q64E mutant was difficult. However, a single crystal, diffracting to 2.51 \AA , could be obtained from which data of limited quality could be collected. Structure solution and refinement provided a view of the site of mutation (data not shown). The carboxylic acid side chain of E64 makes potential hydrogen bonds, with the backbone -NH of Gly76 of the other subunit and with backbone carbonyl (-CO) groups of Lys12 and Phe42 of the same subunit. These are comparable to the hydrogen bonds observed in the cases where Gln is in the position 64 (Fig. 9). The Q64N mutant shows a significant fall in activity at pH values > 8 with a transition that probably corresponds to changes in the ionization state of the catalytic Lys12 residue. Attempts to obtain diffracting quality crystals of Q64N mutant proved futile. To assess the possible structural consequences of the Q to N mutation, the Asn side chain was modelled at position 64 in the structure of the wild-type enzyme (Fig. 10). Of the seven Asn side-chain rotamers in the Coot library [35,36]; three rotamers showed unfavourable steric contacts with neighbouring atoms (rotamers 2, 3 and 6). The modelled structures of the remaining four rotamers (rotamers 1, 4, 5 and 7) are shown in Fig. 10. In all cases, the residue 64-Lys12 side chain-backbone hydrogen bond is no longer present. Of the three key hydrogen-bond contacts made by the Gln residue at position 64 in the wild-type enzyme, only one, the side chain-backbone hydrogen bond to the -CO group of Phe 42, is maintained in three of the rotamers (rotamer 1, 5 and 7). Replacement of Gln by Asn at position 64 is thus likely to weaken the dimer interface because of the absence of the hydrogen bond to Gly76 -NH of the neighboring subunit. Further, the loss of the hydrogen bond to the Lys12 backbone -CO may have an influence on activity. It may be noted that, in all native TIM structures, Lys12 is held in an

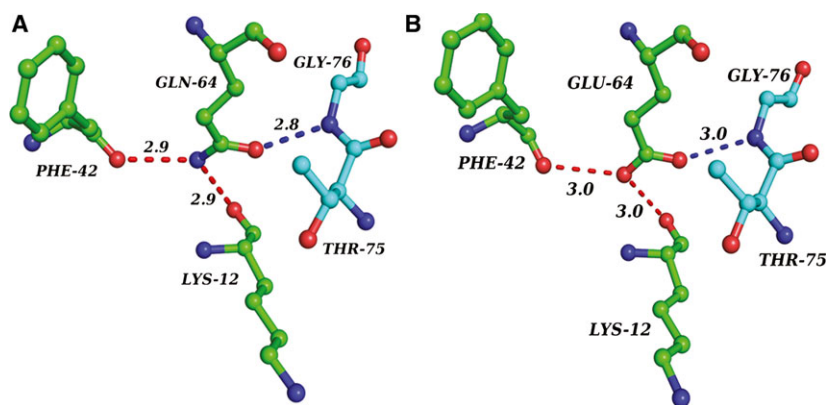


Fig. 9. Comparison of the hydrogen-bonding interactions near the residue 64 in (A) *Pfl*TIM wild-type (PDB code: [1O5X](#)) and (B) Q64E mutant (PDB code: [5BRB](#)).

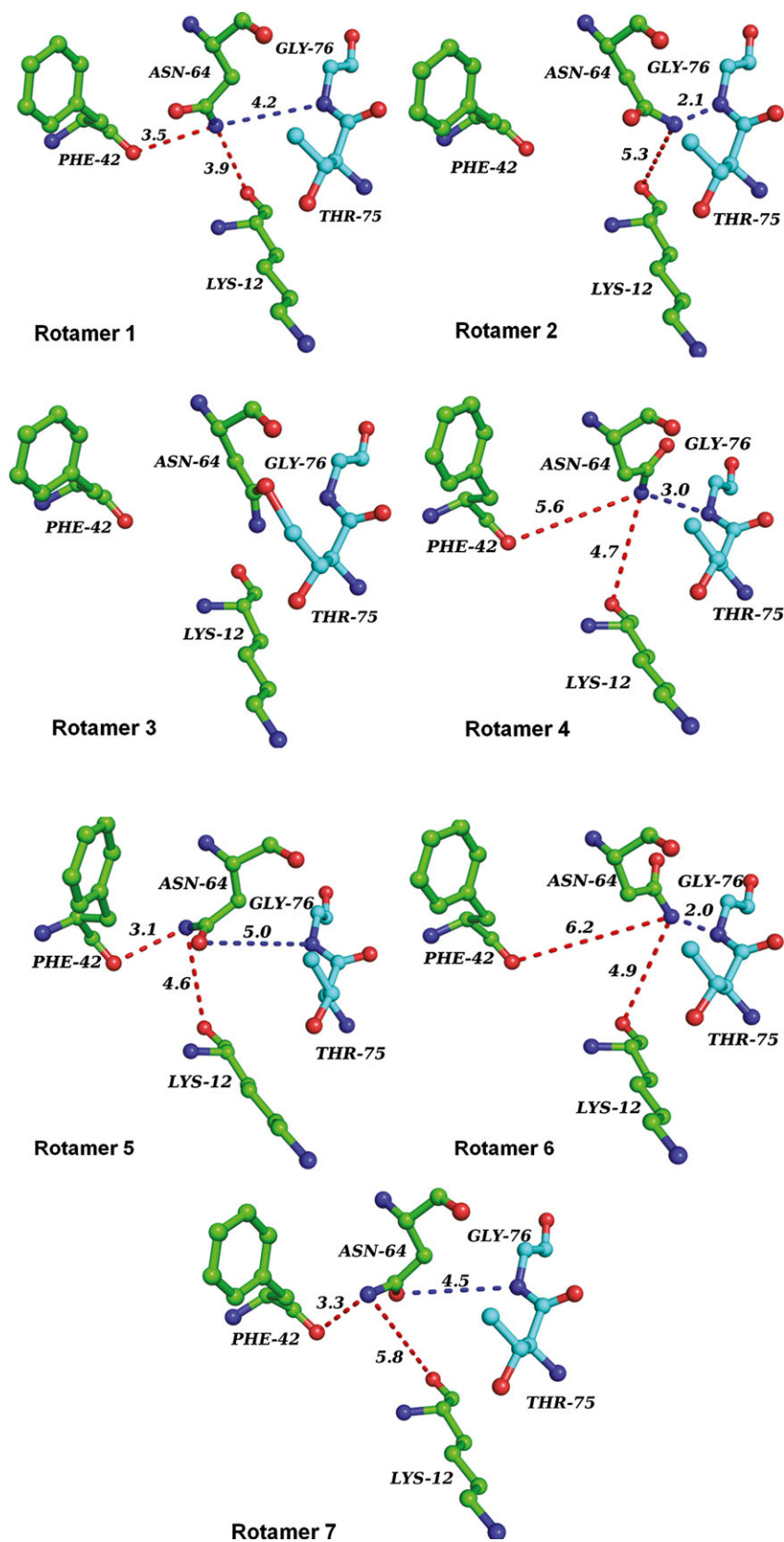


Fig. 10. Possible rotamers of modelled Q64N on *Pf*TIM wild-type structure (PDB code: [1O5X](#)).

unusual backbone conformation ($\phi = 54.3 \pm 5.5$ and $\psi = -144.1 \pm 7.0$) [37]. This strained conformation is stabilized by hydrogen bonds formed by the flanking peptide units with proximal side chains. Our experimental studies, detailed above, suggest a significantly weakened dimer interface in the Q64N mutant resulting in concentration dependence of enzyme activity and dissociation under gel filtration conditions. The Q64N mutation has a significantly greater destabilizing effect on the dimer than the Q64E mutation. A comparison of the limiting activity obtained at high protein concentration suggests that the Q64N mutant is approximately twice as active as the Q64E mutant. Both mutants exhibit similar activities at low pH values, suggesting that ionization of the E64 side chain in the Q64E mutant probably disrupts the local conformation of the active site residues as a result of the loss of the hydrogen-bond interactions described above.

Structural analysis of Thr75 mutants

Diffraction quality crystals were obtained for the four mutants: T75S, T75V, T75C and T75N. Structures were determined at a resolution of 1.80, 1.86, 1.80 and 1.80 Å, respectively. Details of the diffraction data, structure solution and refinement statistics for T75S/V/N/C mutants are provided in Table 2. In all cases, unliganded dimeric structures were obtained with the active site loop 6 occurring in the open form. In all four T75 mutant structures, the active site was occupied by a molecule of ethylene glycol, which was used as a cryoprotectant. The active site geometries for all four mutants were almost identical (Fig. 11). Thr75 lies at the dimer interface making hydrogen-bond contacts with residues from the neighboring subunit. An examination of B-factor plots for the wild-type enzyme and the Thr75 mutants did not reveal any significant differences for the loop residues in the vicinity of the site of mutation. Figure 12 compares the environment of residue 75 in the structure of the wild-type enzyme and three mutants: T75V, T75S and T75N. In the serine mutant, the primary hydroxyl group of the side-chain forms hydrogen bond to the side-chain -CO of Asn10 and side-chain carboxylic group of Glu97 in a manner similar to that observed with Thr at this position. In the T75V mutant, both these inter-subunit hydrogen bonds are lost and are replaced by van der Waals contacts to the side chains of Asn10 and Glu97. The valine side chain takes up an orientation almost identical to that observed for Thr. The largest changes in dimer interface interactions are observed for the T75N mutant. In this case, the hydrogen bond to Glu 97 is lost but a new hydrogen bond between the side-chain

-NH₂ of Asn75 and backbone -CO of Glu64 is observed. In the T75C mutant, the electron density near the site of mutation was poor, preventing the building of a good structural model. These structural results suggest that mutations at position 75 cause relatively small perturbations confined to local structure. Despite the proximity of Thr75 to the active site residues Lys12 and Glu97, the relative orientations of these residues remain unchanged in all the mutants. The biophysical studies described earlier established that the dimer integrity is undiminished upon replacement of Thr (T) 75 by S, V, C and N. The T75S, T75V and T75C mutants exhibit enzyme activities very close to that obtained for the wild-type enzyme. Only the T75N mutant shows a fourfold reduction in activity (Table 1). A comparison was made between the structures of T75N and the wild-type enzyme, T75S and T75V, around the site of mutation. This analysis provided an explanation for the diminished activity of the T75N mutant. In the TWT structure, the oxygen atom (-O^γ) of the Thr side chain makes a close contact with the -C^γH₂ of the active site K12 side chain (O—C; 3.7 Å). In the T75S mutant, the corresponding distance between Ser -O^γ and Lys -C^γH₂ is 3.6 Å, whereas, in the T75V mutant, the contact distance between Val -C^γH₃ and Lys -C^γH₂ is 3.4 Å. In contrast, in the T75N mutant, the shortest distances between the atoms of N75 side chain and Lys12 are 4.6 Å (N75 side-chain -CO and K12 side-chain -C^γH₂) and 4.7 Å (N75 -C^βH₂ and K12 side-chain -C^γH₂) (Fig. 13). The poorer packing of the K12 side chain with the proximal N75 residue may contribute to greater conformational flexibility, resulting in marginally diminished activity. The accommodation of as many as four diverse residues at position 75 with relatively limited effects on structure and activity raises important questions. Why is Thr (T) 75 completely conserved in the very large dataset of bacterial TIM sequences and, indeed, in all of the available archaeal and eukaryotic sequences? What is the phenotype that imposes a strong constraint on the residue selected at this site? In order to further understand the possible reasons for conservation of Thr (T) 75 residue, we aimed to determine the temperature dependence of enzyme activity, as discussed below.

Temperature dependence of enzyme activity in Thr (T) 75 mutants

Figure 14A shows the change in specific activity as a function of temperature for the wild-type enzyme and the mutants T75S and T75N. The temperature dependence determined for the T75V and T75C mutants are very similar to that observed for T75S (data not

Table 2. Crystallographic data collection and refinement statistics. Values given in parenthesis are for the highest resolution shell.

Mutant proteins	T75S	T75V	T75N	T75C	Q64E
PDB code	4ZZ9	5BMW	5BMX	5BNK	5BRB
Space group	P2 ₁	P2 ₁	P2 ₁ 2 ₁ 2 ₁	P2 ₁	P2 ₁
Unit cell					
<i>a</i> , <i>b</i> , <i>c</i> (Å)	39.23,76.54, 74.94	39.21,76.02, 74.36	50.64,106.72, 179.62	39.36,76.88, 74.48	39.02,75.35,74.13
β(°)	98.27	97.47	90	97.79	97.72
Resolution (Å)	38.82–1.80 (1.90–1.80)	38.88–1.86 (1.96–1.86)	30.58–1.80 (1.90–1.80)	33.26–1.80 (1.90–1.80)	73.46–2.51 (2.65–2.51)
Number of observed reflections	174 650 (23 676)	203 849 (27 042)	668 294 (80 908)	167 317 (24 014)	45 770 (5215)
Number of unique reflections	40 317 (5839)	36 392 (5211)	88 535 (12379)	40 771 (5902)	14 204 (1734)
Redundancy	4.3 (4.1)	5.6 (5.2)	7.5 (6.5)	4.1 (4.1)	3.2 (3.0)
Completeness (%)	99.9 (99.5)	99.8 (98.4)	97.2 (94.6)	100.0 (100.0)	97.2 (81.4)
Overall <i>R</i> _{merge} (%)	0.100 (0.480)	0.056 (0.156)	0.116 (0.297)	0.058 (0.593)	0.153 0.(441)
Mean (<i>I</i> /σ <i>I</i>)	10.1(2.8)	22.2(9.8)	11.3(4.8)	12.6(2.2)	5.6(2.3)
<i>R</i> _{work} / <i>R</i> _{free}	0.175/0.237	0.131/0.182	0.167/0.216	0.216/0.258	0.229/293
Model quality					
Number of atoms	4382	4411	8651	3827	3732
Number of water molecules	525	483	931	273	62
Wilson B-factor	17.7	13.1	10.3	24.8	40
Average B-factor (Å ²)	15.6	11.6	15.7	29.8	23.6
Protein	13.6	9.8	13.2	30.7	24.8
Water	24.9	23.6	26.3	43.5	18.1
rmsd bond lengths (Å)	0.018	0.019	0.02	0.018	0.007
rmsd bond angles (°)	1.76	1.8	2.01	1.84	1.07
Ramachandran map (%)					
Most favored (%)	94.4	94.9	94.9	95.2	93.4
Additionally allowed (%)	5.1	4.6	4.8	4.8	6.4
Generously allowed (%)	0.4	0.4	0.3	0	0.2
Outliers (%)	0	0	0	0	0

shown). In the case of TIM wild-type (TWT), there is a steady increase in the specific activity in the range 25–45 °C, with a levelling off observed at 50 °C. At higher temperatures, the enzyme begins to precipitate. This temperature-dependent increase in activity is generally observed for enzymes and has been the subject of recent discussion [38]. In contrast to the wild-type enzyme, the T75S mutant shows a very small increase in activity over the range of 25–40 °C and a sharp fall in activity at higher temperatures, with > 50% loss of activity at temperatures > 45 °C. The T75N mutant exhibits a completely different temperature dependence, with > 50% reduction of activity even at 30 °C. In all the cases, the assays were carried out by incubating a stock protein solution at a given temperature for 4 min, followed by the addition of an aliquot of protein to a pre-equilibrated assay mixture to initiate the reaction. Precipitation of the protein is minimized under these conditions.

In a separate set of experiments, a stock enzyme solution was incubated for 45 min at the desired tempera-

tures, followed by centrifugation and removal of precipitated protein and subsequent addition of an aliquot from the supernatant to the assay mixture maintained at 25 °C. A plot of the activity as a function of temperature following this protocol is provided in Fig. 14B. In this case, the mutants T75V/N and T75S show a dramatic fall in activity at temperatures between 35 °C and 40 °C, whereas the fall in activity for the T75C mutant is pronounced at temperatures close to 45 °C. The wild-type enzyme exhibits substantial activity even at 45 °C with precipitation and loss of activity being observed only at temperatures > 45 °C. These results demonstrate that while the T75 mutants show little or no loss of activity compared to the wild-type enzyme at 25 °C, there is a pronounced diminution of activity at temperatures in the range 30–45 °C.

Discussion

A relatively small number of residues are completely conserved in enzyme sequences when large datasets

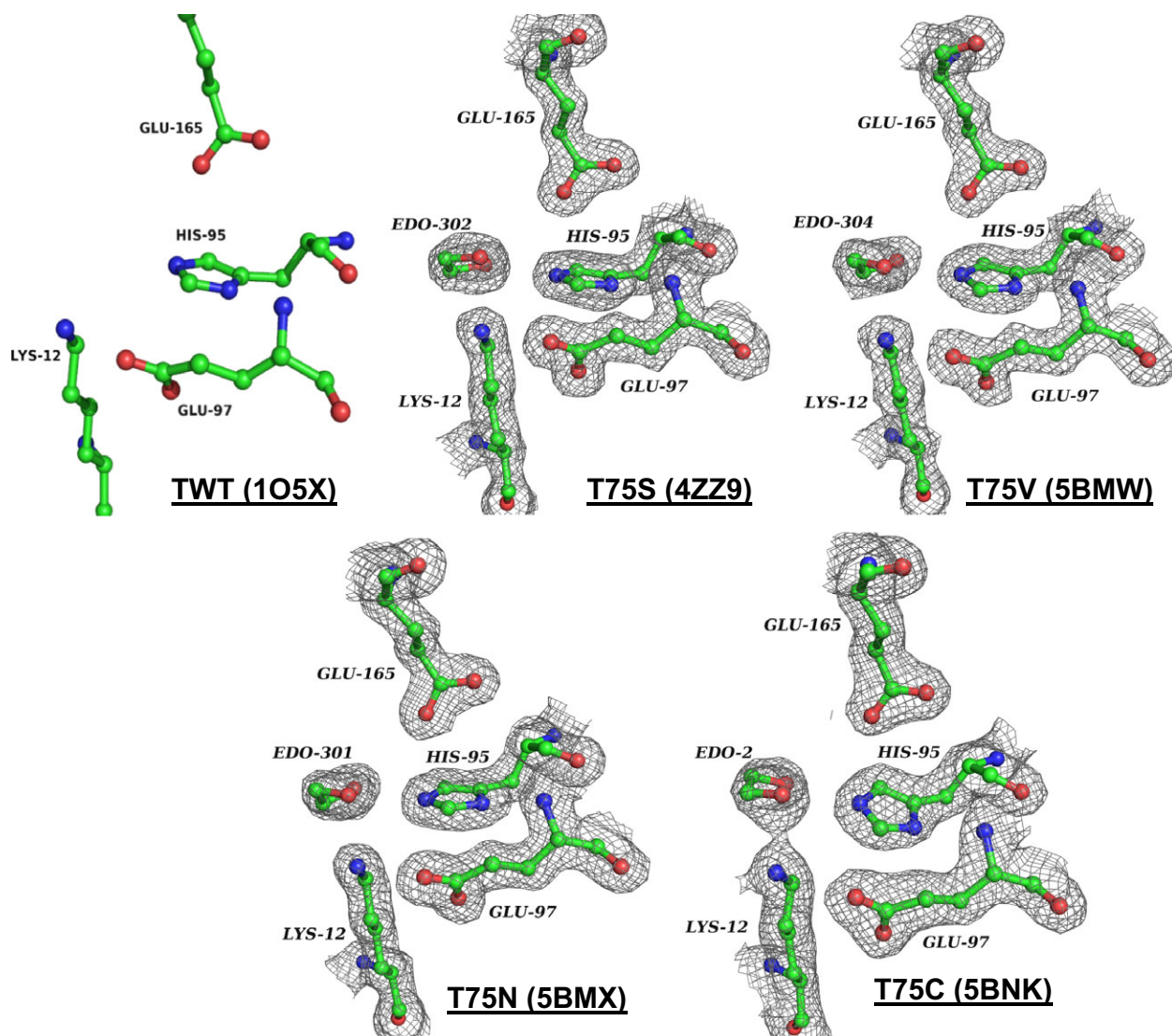


Fig. 11. Electron density maps ($2F_o - F_c$, contoured at 1σ) at the active site residues in *PftIM* wild-type ([1O5X](#)), T75S ([4ZZ9](#)), T75V ([5BMW](#)), T75N ([5BMX](#)) and T75C ([5BNK](#)) structures.

from diverse organisms are examined. In the case of TIM, as few as ten residues are completely conserved in sequences that have a length distribution between 220 and 270 residues. Of the ten conserved residues, four Lys (K) 12, His (H) 95, Glu (E) 97 and Glu (E) 165 are positioned in close proximity to the substrate and have been implicated in the proton transfer reaction [6,10–12]. The remaining six conserved residues T75, C126, P166, G209, G210 and G228 do not have a direct role in the catalytic process, although they are undoubtedly critical for maintaining the structural integrity of the active site and in permitting key dynamic processes that may be important for achieving key catalytic efficiency. C126 lies proximal to the

active site residue E165. Although this fully conserved residue is not involved in inter-subunit interactions, it is mainly important for stability and proper folding of the dimer [5,39,40]. P166 is a critical residue in the N-terminal hinge that controls the opening and closing movement of active site loop 6, which is crucial for substrate sequestration and subsequent product release [41–44]. G209 and G210 are part of the important highly conserved 208–211 segment that undergoes a peptide flip on going from unliganded to liganded structure. This helps in the movement of catalytic loop 6 allowing catalytic base E165 to attain a conformation necessary for TIM activity. The flip of 209–210 and 210–211 also helps S211 to form a crucial

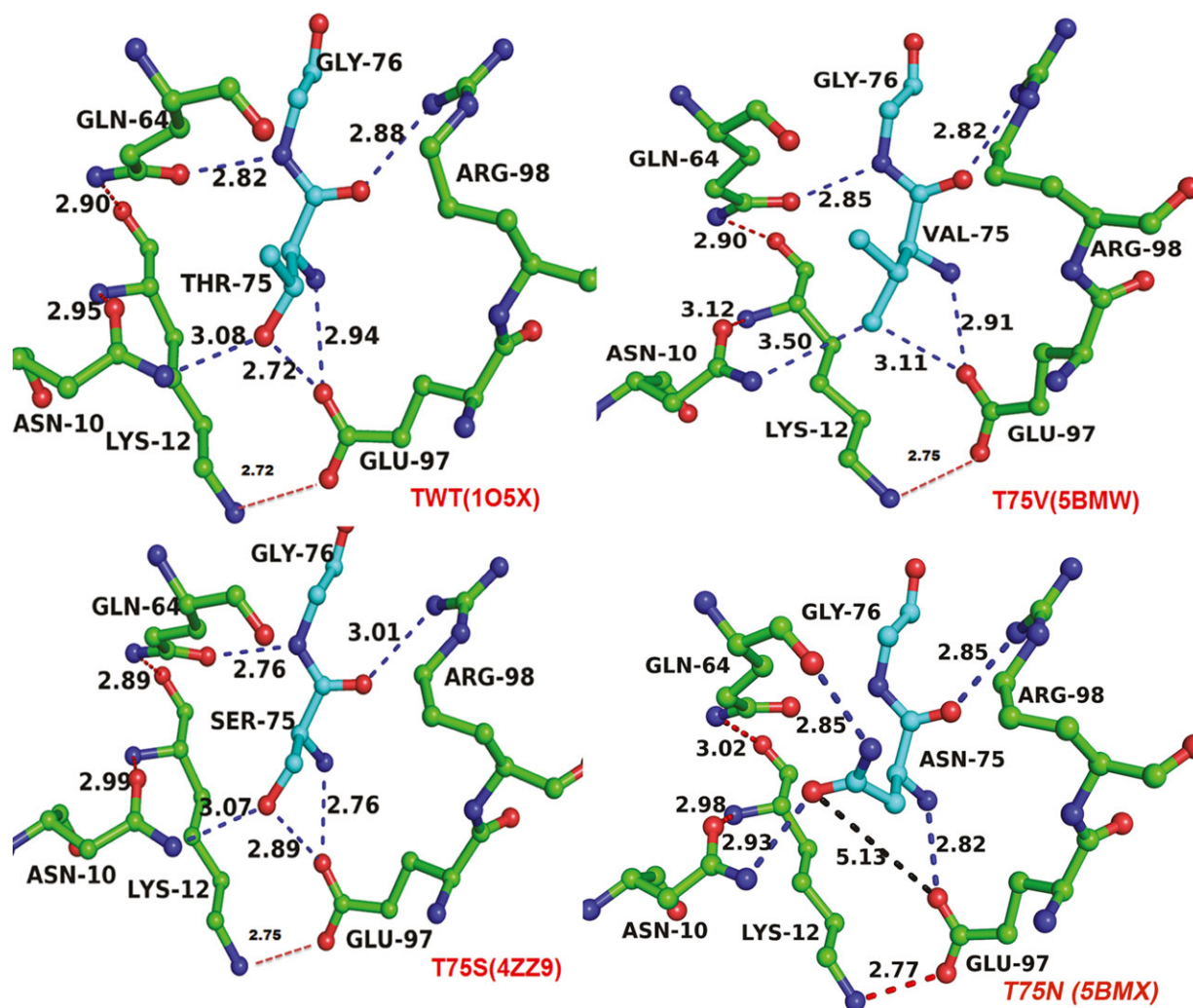


Fig. 12. Comparison near the site of mutation (position 75) in TWT ([1O5X](#)) and the three T75 mutants [T75S ([4ZZ9](#)), T75V ([5BMW](#)) and T75N ([5BMX](#))]. The PDB entries are given in parenthesis. Inter-subunit hydrogen-bonding interactions are shown in blue and intra-subunit H-bonding interactions are shown in red.

interaction with the phosphate moiety of the substrate in the liganded state [analysis performed with the help of yeast TIM structures, Protein Data Bank (PDB) code: [1NEY](#) and [1YPI](#)]. G228 helps in appropriate positioning of the 208–209 segment of the aforementioned 208–211 segment by a backbone-backbone hydrogen bond (G228 -CO and Y208 -NH). The backbone torsion angles adopted by this residue are stereochemically feasible only for a Gly residue ($\varphi = 147.1$, $\psi = -161.9$, in [1NEY](#)) [45].

In the present study, we have examined the consequences of mutation of the T75 residue. In addition to complete conserved position in enzymatic sequences, there are a limited number of sites at which very few residues appear to be accommodated in natural sequences. Position 64 in TIM (i.e. the numbering

scheme used corresponds to that for the yeast and the *Plasmodial* enzymes) is one such site where, of the 3398 sequences examined, an overwhelming majority have Gln (Q) (3011/3398), whereas a smaller but significant number have Glu (E) (383/3398), a conservative substitution, at this position. These observations clearly suggest that a strong selective pressure operates to limit amino acid variability at position 64. Inspection of the three-dimensional structures of TIM from different sources establishes that both residues lie close to the active site and participate in a network of intra and inter-subunit hydrogen-bond interactions. Thr75 lies near the TIM active site at the dimer interface making key contacts with N10 and E97 of the other subunit. N10, in turn, makes an important hydrogen bond to the K12 backbone -NH, which is presumably

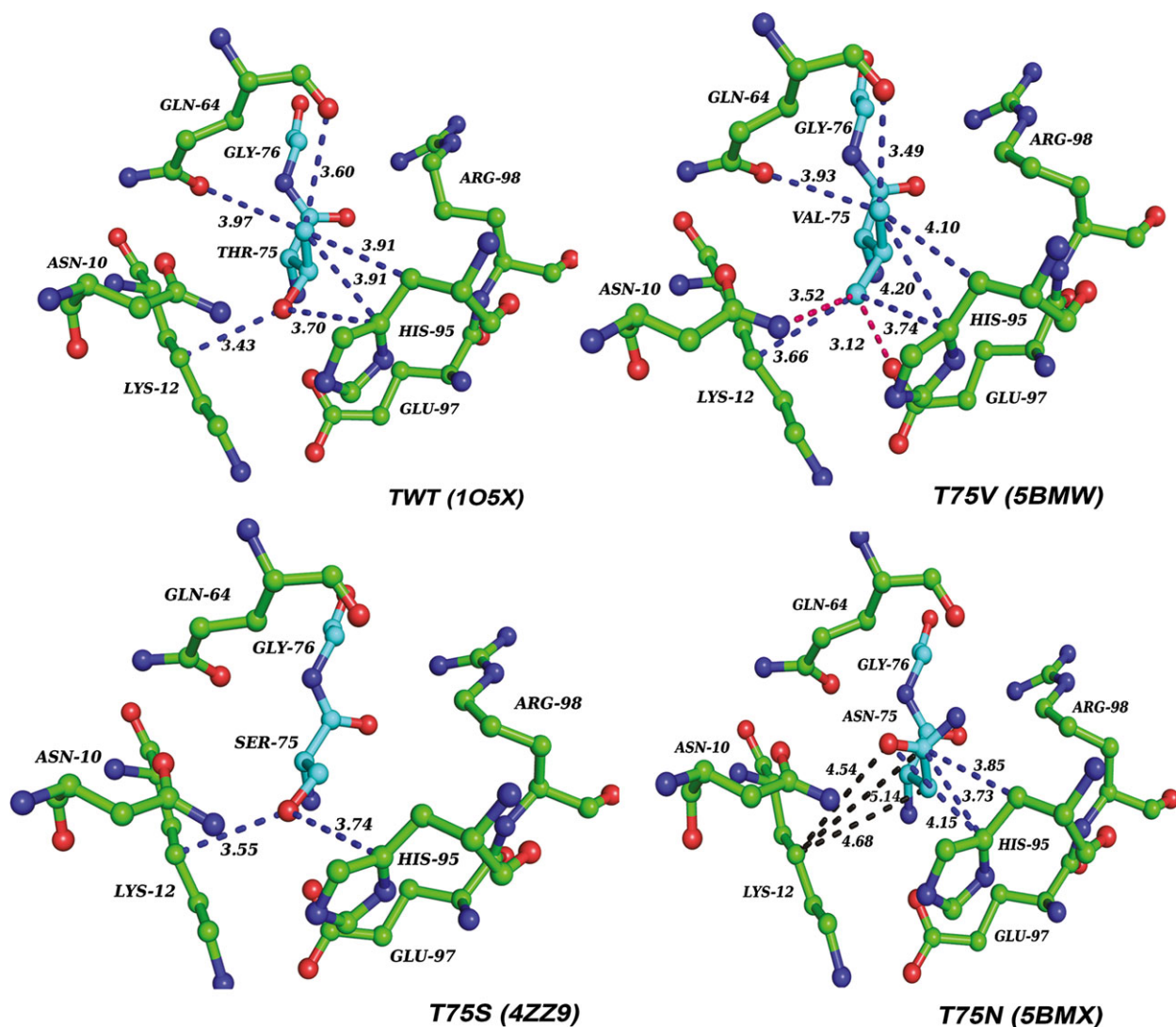


Fig. 13. Comparative view of the van der Waals interactions in *PfTIM* wild-type (PDB code: [1O5X](#)), T75S (PDB code: [4ZZ9](#)), T75V (PDB code: [5BMW](#)) and T75N (PDB code: [5BMX](#)) mutants. Similar interactions present in TWT and the mutants are shown in blue; new van der Waals interactions as a result of the mutations are shown in red; interactions that are lost as a result of the mutations are shown in black.

essential for maintaining the unusual conformation of this key residue [37]. E97 interacts directly with the side-chain amino group of K12 and may contribute to the proton transfer process [6]. We therefore anticipated that replacement of T75 may result in both destabilization of the TIM dimer and/or impaired activity. The Q64 side chain makes an important hydrogen bond to the backbone -CO of K12 and an inter-subunit hydrogen bond to the backbone -NH of G76, which flanks the Thr75 residue. In this case also, mutational replacement might be expected to affect dimer stability and/or enzyme activity. The results reported in the present study establish that mutations at position 75 (T75S, T75V, T75C and T75N) do not

appreciably affect dimer stability. Spectroscopic studies establish that these substitutions have little effect on the overall structure of the enzyme, a conclusion that is supported by the observation of intact dimers in the crystal structures of T75S, T75V and T75N. Indeed, the active site geometries in the mutant structures are almost identical to that observed in the wild-type enzyme. Elution profiles of these mutants in gel filtration studies are similar to TIM wild-type (TWT), while measured enzyme activities are also very similar to those obtained for TWT, with a marginal fall observed for the T75N mutant. Why then is T75 conserved? Examination of the temperature dependences of enzyme activity in the range 25–50 °C reveals that the

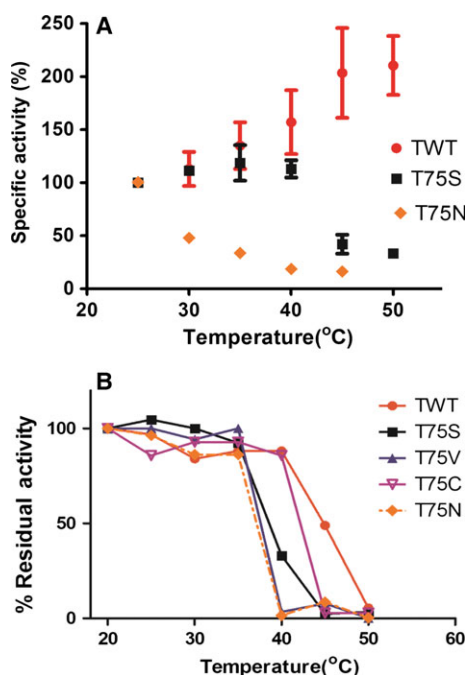


Fig. 14. (A) Temperature dependence of specific activity for T75 mutants. (B) Residual activity at different temperatures. In each case, a protein concentration of 1 μM was used in the presence of a substrate concentration of 3 mM .

wild-type enzyme shows a steady increase in activity with temperature up to 45 °C, whereas all four mutants show a dramatic fall in activity in the range 35–45 °C. All the T75 mutants were significantly less stable in the presence of high concentration of urea. While TIM wild-type remains unaffected by concentrations of urea as high as 6 M , all the T75 mutants unfold at urea concentrations in the range 3.5–4 M . These results point to the possibility that temperature stability in this range may be the phenotype being selected, rendering position 75 resistant to evolutionary drift.

The Q64E and Q64N mutants display a significant destabilization of the TIM dimer, as evidenced by the gel filtration elution profile and concentration dependence of enzyme activity in the range 5–150 nM . In addition, both mutants show a loss of near UV-CD bands and enhanced binding of the fluorescent probe ANS, establishing significant perturbation of the tertiary structure in the vicinity of the site of mutation. Both mutants also unfold at relatively low concentrations of urea (3.5–4 M) in contrast to the wild-type enzyme, which remains stable even at significantly higher urea concentrations. The concentration dependence of enzyme activity has been used to estimate the dissociation constant for the Q64E and Q64N mutant dimers, yielding values of $44.6 \pm 8.4 \text{ nM}$ and

$73.7 \pm 9.2 \text{ nM}$, respectively. These are significantly higher than the estimated values for the TIM wild-type enzyme from different organisms. The value of 0.00001 nM was estimated by Lolis *et al.* [33] on the basis of the buried surface area in the crystallographically determined dimer structure of yeast TIM; the value of 0.01 nM was estimated by Rietveld *et al.* [34] by calculating the Gibbs free energy change of dissociation as a result of GdnHCl-induced denaturation of rabbit muscle TIM [34]. Using these lower (0.00001 nM) and upper (0.01 nM) limits of K_d for dimerization of wild-type enzyme from the above studies, the Gibbs free energy changes upon mutation ($\Delta\Delta G$) of 5.2–9.2 $\text{kcal}\cdot\text{mol}^{-1}$ are estimated for Q64N, while the corresponding values for the Q64E mutant are 4.9–8.9 $\text{kcal}\cdot\text{mol}^{-1}$. These $\Delta\Delta G$ values are broadly compatible with the loss of hydrogen-bond interactions upon mutational replacements together with concomitant changes in local packing (van der Waals) interactions. The Q64E mutant displays a pronounced pH dependence of activity, with a dramatic fall in the range pH 7 to pH 8. This is distinct from the behaviour of the wild-type enzyme, which shows a broad range of unimpaired activity between pH 7 and pH 9. The titration of the buried glutamate residue in the Q64E mutant must contribute to the structural alterations that influence the orientation of catalytic residues. This indirect effect on the observed pH dependence of enzyme activity has long been an important factor that prevents meaningful interpretation of the $\text{p}K_a$ of groups directly involved in catalytic reactions in enzymes [46]. The influence of this buried glutamic acid on the stability of the TIM from *L. mexicana* has been demonstrated previously. In that case, the wild-type enzyme contains a Glu (E) residue at position 65 (equivalent to position 64 in the yeast and *Plasmodial* sequences). As noted earlier, the E65Q mutation in this case results in a dramatic enhancement of the thermal stability of the enzyme [26,47], while, in the present study, the thermal stability of the mutant structure has diminished as a result of mutation at the sites 64 and 75, as monitored by CD spectroscopy.

The small number of fully conserved and highly conserved residues in a large dataset of TIM sequences suggests that the mutational substitutions are well tolerated at most positions in the polypeptide sequence. The inference that there are multiple sequence solutions to the problems of folding and construction of protein–protein interfaces appears to be reasonable. In contrast, the constraints of catalytic chemistry impose a unique sequence solution or a restricted set of solutions for residues directly involved in the catalytic pro-

cess and others that form the immediate scaffolding. In the case of TIM, all the fully conserved residues are proximal to the active site and highly conserved residues, such as Q64, interact directly with the active site residues. Selective pressures undoubtedly shape TIM sequences, optimizing specific features such as temperature dependence of activity and the dissociation constants of the dimer, parameters that assume considerable importance as the integrity of the active site is inextricably linked to the integrity of the structure of the protein dimer.

Experimental procedures

Cloning expression and purification

The TIM gene from the organism *Pf* has been cloned into the expression vector pTrc99A, known as pARC1008 [48]. The protein was overexpressed into a host TIM null mutant *Escherichia coli* strain AA200 [49]. To probe the role of residue 64 and 75, mutagenesis was carried out in the *Pf* TIM gene by site-directed mutagenesis using single primer method as described previously [50]. The absence of an appropriate restriction site necessitated a two-step procedure to generate mutants at the two sites. In the first step, two intermediate clones at each position were generated (Q64int and T75int mutants). This was carried out using the wild-type gene as template and using the single primers with *EcoRV* restriction sites (primers shown in Table S1). The generated clones were confirmed by restriction digestion. In the second step, mutant clones Q64N, Q64E and T75S, T75V, T75C and T75N were constructed, with the subsequent removal of the restriction site of *EcoRV* and the introduction of the desired mutations, using the Q64int and T75int clone gene as the template for PCR.

For both PCRs, the thermostable proofreading polymerase enzyme *Phusion* (Thermo Scientific, Waltham, MA, USA) was used. The PCR cycling conditions involved an initial step at 95 °C for 5 min followed by 40 cycles consisting of 1 min at 95 °C, annealing at 50 °C for 1 min and extension at 72 °C for 10 min. Final incubation at 72 °C for 20 min was applied. The presence of mutations was confirmed by restriction digestion and DNA sequencing. The primers used to generate the two Q64 and four T75 mutants are shown in Table S1. The mutant TIM genes, cloned into the expression vector pTrc99A, were expressed in *E. coli* AA200 (devoid of inherent bacterial TIM gene) strain. The cells were grown in Terrific broth (containing 100 µg·mL⁻¹ antibiotic ampicillin) at 37 °C. The cells were induced with 400 µM IPTG at OD₆₀₀ of 0.6–0.8, followed by harvesting using centrifugation (7245 g for 20 min at 4 °C). Later, the cells were resuspended in lysis buffer containing 20 mM Tris-HCl (pH 8.0), EDTA (1 mM), PMSF

(0.01 mM), DTT (2 mM) and 10% glycerol and disrupted by sonication. After centrifugation (19 320 g for 30 min at 4 °C) and removal of the cell debris, the supernatant was fractionated with ammonium sulfate. The protein fractions, containing T75 mutants, were in the supernatant solution of 60% ammonium sulfate saturation. The supernatant was thoroughly dialyzed against 20 mM Tris-HCl (pH 8.0) buffer solution. The dialyzed solution was centrifuged (19 320 g for 45 min at 4 °C) and the soluble fraction was further purified by anion exchange (Q-Sepharose; GE Healthcare UK Ltd, Little Chalfont, UK) chromatography, with a linear gradient of NaCl (0–1 M) salt [5]. On the other hand, the almost pure Q64 mutants remained in the supernatant of 80% ammonium sulfate saturation (first step: 40% and second step: 80% ammonium sulfate precipitation to the supernatant of 40% precipitation). The purified protein obtained was then extensively dialyzed against 20 mM Tris-HCl (pH 8.0) at 4 °C for desalting. Protein purity was checked by 12% SDS/PAGE. The masses of the mutant proteins were confirmed by LC-ESI-MS with a Bruker Q-TOF mass spectrometer (Bruker Instruments, Inc., Billerica, MA, USA), Mass_{obs} (Mass_{calc}): 27831.3 Da (27831.5 Da) TWT; 27818.2 Da (27817.8 Da) T75S; 27828.7 Da (27829.6 Da) T75V; 27832.6 Da (27833.6 Da) T75C; 27844.4 Da (27844.6 Da) T75N; 27817.8 Da (27817.5 Da) Q64N and 27833.3 Da (27832.5 Da) Q64E (data not shown). Protein concentrations were determined by Bradford's method using BSA as the standard [51] and are expressed (µM or nM) using the monomer molecular mass.

Size exclusion chromatography

Size exclusion chromatography was performed using a Superdex-200 column (length 300 mm, internal diameter 10 mm) (GE Healthcare) for Q64 mutants and a Superdex-75 column (length 300 mm, internal diameter 10 mm) for T75 mutants, attached to an AKTA Basic FPLC system at a flow rate of 0.5 mL·min⁻¹. The solvent system was 20 mM Tris-HCl (pH 8.0). Protein elution was monitored at a wavelength of 280 nm. The column was calibrated with BSA (66 kDa) and carbonic anhydrase (29 kDa). All the chromatographic runs were performed at 25 °C.

CD

Far UV and near UV-CD measurements were carried out on a Jasco-815 spectropolarimeter (Jasco Inc., Easton, MD, USA) connected to a thermostatted cell holder, which was temperature controlled inside the cuvette with a Peltier device. Denaturation studies were performed by incubating 5 µM protein with various concentrations of urea for 45 min and spectra were recorded in the range 250–200 nm and averaged over three scans. For thermal melting studies, far UV-CD spectra were recorded over the range 20–75 °C

at intervals of 5 °C. At each temperature, the protein was incubated for 10 min to follow the unfolding transition. A cuvette of path length of 1 mm and a protein concentration of 15 µM were used. The spectra were averaged over three scans at a scanning speed of 10 nm·min⁻¹. The change of ellipticity was measured as a function of temperature for thermal melting. Individual spectra (far UV-CD: 250–200 nm; near UV-CD: 300–250 nm) were averaged over four scans with the same scan speed. All experiments were carried out in 20 mM Tris-HCl (pH 8.0).

Fluorescence spectroscopy

Emission spectra were recorded on a spectrofluorimeter (Hitachi-F-2500; Hitachi, Tokyo, Japan). For denaturation studies, the protein samples were excited at 295 nm and the emission spectra were recorded in the range 300–400 nm ($\lambda_{\text{excitation}} = 295$ nm) after incubating 2 µM of each protein with different concentrations of urea for 45 min. Excitation and emission band passes were kept at 5 nm and 10 nm, respectively for the Q64 mutants, whereas they were both set at 5 nm for the T75 mutants. For the ANS binding study, 5 µM of TIM wild-type and both the Q64 mutants were incubated with different concentrations of ANS and excited either at 280 nm or at 370 nm and emission spectra were recorded in the range 300–600 nm and 400–600 nm, respectively.

Enzyme activity

The kinetics of the conversion of GAP to dihydroxyacetone phosphate (DHAP) by the enzyme TIM (*Pf* wild-type and mutants) was monitored in the presence of coupling enzyme, α -glycerol phosphate dehydrogenase, as described by Plaut and Knowles [52]. The final 500-µL reaction mixture contained 100 mM TEA (pH 7.6), 0.1 mM NADH, 5 mM EDTA, 10 µg of the α -glycerol phosphate dehydrogenase and varying concentrations (0.25–4.5 mM) of the substrate (GAP) to which TIM was added to initiate the reaction. In case of the Q64 mutants the aforementioned assay technique gave a two-phase reaction profile (data not shown). The two-phase assay profiles for the Q64 mutants occurred probably as a result of perturbation in dimer–monomer equilibrium as a result of sudden dilution of the stock solution. Knowles' protocol has been slightly modified in the present study, which is the first to achieve the dimer–monomer equilibrium and then monitor the enzyme kinetics. For this, the *Pf* wild-type and Q64 TIM mutants were incubated for 45 min in the assay mixture and then the reaction was monitored by adding the substrate GAP. *Pf*TIM wild-type, TWT (14 ng), Q64N (120 ng) and Q64E (300 ng) were used for substrate titration in accordance with the Knowles protocol, whereas, for the concentration- and pH-dependent experiments, the alternate protocol was used. The progress of the reaction was monitored by the

decrease in absorbance of NADH at 340 nm. The extinction coefficient of NADH was taken to be 6220 M⁻¹·cm⁻¹ at 340 nm [53]. In the range studied, the linear dependence of the initial rate on the enzyme concentration ensures the validity of the assay [52]. The values for the kinetic parameters of T75 mutants (K_m , k_{cat}) were determined by fitting the initial velocity data to the Michaelis–Menten equation using PRISM, version 5. For this experiment, 14 ng of *Pf*TIM wild-type and T75S/V/C mutants and 28 ng of T75N mutant were used. The kinetic parameters for Q64 could not be determined because of the absence of saturation at higher concentrations of substrate. As a result, the specific activities at a particular substrate concentration were compared. Activities of all the mutants and of wild-type were measured as a function of protein concentrations at ambient temperature (23 °C). Concentrations varied in the range 0.15–5 nM in presence of 3 mM substrate for the T75 mutants and wild-type TIM, whereas, for the less active Q64 mutants, the concentrations varied in the range 5–200 nM. The effect of temperature on the activity of T75 mutants was also measured by monitoring the reaction at different temperatures, as well as by incubating the protein at 28 µM at different temperatures and then diluting it to 1 nM at room temperature for measuring residual activity. A concentration of 100 mM of mixed Tris HCl-MES-acetate-glycine buffer of different pH values (ionic strength = 0.1) was used for pH dependence of the specific activity of Q64 mutants.

Crystallization and X-ray diffraction data collection of *Pf*TIM T75 and Q64 mutants

The Q64 and T75 mutants were crystallized by the hanging drop method at 23 °C [54]. The concentrations of the two mutant proteins were 1.5 and 10 mg·mL⁻¹, respectively. The unliganded T75S crystal was obtained under the conditions: 22% poly(ethylene glycol)-1450, 100 mM HEPES buffer (pH 7.0), 10 mM calcium chloride, 0.5 mM EDTA; the unliganded T75V crystal was obtained under the conditions: 20% poly(ethylene glycol)-1450, 100 mM MES buffer (pH 6.5), 10 mM calcium chloride, 0.5 mM EDTA; the unliganded T75N crystal was obtained under the conditions: 28% poly(ethylene glycol)-1450, 100 mM Tris-HCl buffer (pH 8.0), 10 mM lithium sulfate, 0.5 mM EDTA; and the unliganded T75C crystal was obtained under the conditions: 16% poly(ethylene glycol)-1450, 100 mM HEPES buffer (pH 7.5), 10 mM CaCl₂, 0.5 mM EDTA. The hanging drop contained 3 µL of protein and 3 µL of crystallization cocktail equilibrated against 400 µL of crystallization cocktail as the reservoir buffer. The crystals appeared within 4 days and grew to required sizes within 10–15 days. The Q64N and Q64E mutants crystallized under a number of conditions. However, these crystals did not diffract X-rays to useful resolution. The crystal obtained with Q64E mutant diffracted X-rays to a resolution of 2.51 Å only under one of the con-

ditions (28% poly(ethylene glycol)-1450, 100 mM HEPES, pH 7.5, 10 mM CaCl₂).

Diffraction quality crystals obtained under the above mentioned conditions were soaked in 10% (v/v) ethylene glycol solution mixed with the reservoir buffer before flash freezing in liquid nitrogen. X-ray diffraction data for Q64E, T75S and T75V mutants were collected using a RU 200 rotating anode X-ray generator (Rigaku, Tokyo, Japan) ($\lambda = 1.54 \text{ \AA}$). Datasets for T75N and T75C mutants were collected using synchrotron radiation ($\lambda = 0.954 \text{ \AA}$) at the European Synchrotron Radiation Facility (ESRF), Grenoble and on a CCD MARmosaic 225 detector. The unliganded T75S, T75C and T75N crystals diffracted to 1.80 \AA , whereas, the unliganded T75V crystal diffracted to 1.86 \AA . All datasets were processed using MOSFLM [55,56] and scaled with SCALA [57] of the CCP4 (Collaborative Computational Project, Number 4, 1994) software suite [58].

Structure determination and refinement

Structures of all the five mutants were determined with the molecular replacement software PHASER of the CCP4 package [59]. The native *Pf*TIM crystal structure (PDB code: [1O5X](#); 1.1 \AA) was used as the template for structure determination of all the mutants and their complexes, Q64E-unlig, T75S-unlig, T75V-unlig, T75C-unlig and T75N-unlig. The coordinates of 1O5X were modified by removing loop 6 residues, residues near the site of mutations and the regions that interact with it, ligand, water molecules and alternate conformations, before initiating molecular replacement calculations. Refinements of all the structures were carried out using REFMAC5 [60,61], with an initial 20 cycles of rigid body refinement, followed by 100 cycles of restrained refinement. On the basis of the electron density maps, $2F_o - F_c$ and $F_o - F_c$, contoured at 1σ and 3σ , respectively, the loop 6 residues, the residues that were absent in the model, ligand and water molecules, were built. Model building was carried out using COOT [35,36]. Two subunits were present in one asymmetric unit, in the case of the Q64E-unlig, T75S-unlig, T75V-unlig and T75C-unlig structures, whereas, for T75N-unlig, which belonged to a different space group, four subunits were observed. The presence of the Q64E, T75S, T75V and T75N mutations were confirmed from the difference Fourier maps. The T75C mutant structure was not well-defined near the site of mutation as a result of static disorder. Water molecules were automatically located by COOT and accepted if the peak observed was above 1.5σ in a $2F_o - F_c$ map and 3σ in an $F_o - F_c$ map. Alternate conformations of residues were included wherever necessary and the B-factors of all the atoms were refined. All the structures were refined to reasonable R_{work} and R_{free} values and good geometry. The quality of the structures was evaluated by PROCHECK of the CCP4 suite [62]. The electron density maps ($2F_o - F_c$, contoured at 1.0σ) surrounding the residues at position 64 and 75 (data

not shown) for the mutants, confirmed the presence of the mutations. The data collection and refinement statistics for the mutant structures are shown in Table 2. Density for the ligand was not observed in any of the mutant crystal structures, obtained by cocrystallization with the ligand. Images were generated using PYMOL (<http://www.pymol.org>) [63]. The experimental structure factors and the atomic coordinates have been deposited in the PDB.

Acknowledgements

We thank N. V. Joshi for analysis of the TIM sequences and helpful discussions. We also thank the support staff at MBU X-ray facility and beamline scientists at ESRF, Grenoble, for help during data collection. DB was a senior research fellow of the Council for Scientific and Industrial Research, Government of India. Research on TIM was supported under an institutional grant from the Department of Biotechnology (India). X-ray diffraction and MS facilities were supported by program grants from the Department of Science and Technology and Department of Biotechnology (India).

Author contributions

DB carried out all of the experimental work. DB, MRNM, HB and PB were involved in data analysis. DB, MRNM, HB and PB have approved the final version of the manuscript submitted for publication.

References

- 1 Harms MJ & Thornton JW (2013) Evolutionary biochemistry: revealing the historical and physical causes of protein properties. *Nat Rev Genet* **14**, 559–571.
- 2 Guo HH, Choe J & Loeb LA (2004) Protein tolerance to random amino acid change. *Proc Natl Acad Sci USA* **101**, 9205–9210.
- 3 Sullivan BJ, Durani V & Magliery TJ (2011) Triosephosphate isomerase by consensus design: dramatic differences in physical properties and activity of related variants. *J Mol Biol* **413**, 195–208.
- 4 Sullivan BJ, Nguyen T, Durani V, Mathur D, Rojas S, Thomas M, Syu T & Magliery TJ (2012) Stabilizing proteins from sequence statistics: the interplay of conservation and correlation in triosephosphate isomerase stability. *J Mol Biol* **420**, 384–399.
- 5 Samanta M, Banerjee M, Murthy MRN, Balaram H & Balaram P (2011) Probing the role of the fully conserved Cys126 in triosephosphate isomerase by site-specific mutagenesis – distal effects on dimer stability. *FEBS J* **278**, 1932–1943.

- 6 Samanta M, Murthy MRN, Balaram H & Balaram P (2011) Revisiting the mechanism of the triosephosphate isomerase reaction: the role of the fully conserved glutamic acid 97 residue. *ChemBioChem* **12**, 1886–1896.
- 7 Wierenga R (2001) The TIM-barrel fold: a versatile framework for efficient enzymes. *FEBS Lett* **492**, 193–198.
- 8 Cui Q & Karplus M (2003) Catalysis and specificity in enzymes: a study of triosephosphate isomerase and comparison with methyl glyoxal synthase. *Adv Protein Chem* **66**, 315–372.
- 9 Malabanan MM, Amyes TL & Richard JP (2010) A role for flexible loops in enzyme catalysis. *Curr Opin Struct Biol* **20**, 702–710.
- 10 Richard JP (2012) A paradigm for enzyme-catalyzed proton transfer at carbon: triosephosphate isomerase. *Biochemistry* **51**, 2652–2661.
- 11 Richard JP, Amyes TL, Goryanova B & Zhai X (2014) Enzyme architecture: on the importance of being in a protein cage. *Curr Opin Chem Biol* **21**, 1–10.
- 12 Richard JP, Zhai X & Malabanan MM (2014) Reflections on the catalytic power of a TIM-barrel. *Bioorg Chem* **57**, 206–212.
- 13 Albery WJ & Knowles JR (1976) Evolution of enzyme function and the development of catalytic efficiency. *Biochemistry* **15**, 5631–5640.
- 14 Orosz F, Oláh J & Ovádi J (2009) Triosephosphate isomerase deficiency: new insights into an enigmatic disease. *Biochim Biophys Acta* **1792**, 1168–1174.
- 15 Lincet H & Icard P (2015) How do glycolytic enzymes favour cancer cell proliferation by nonmetabolic functions & quest. *Oncogene* **34**, 3751–3759.
- 16 Consortium U (2011) Ongoing and future developments at the Universal Protein Resource. *Nucleic Acids Res* **39**, D214–D219.
- 17 Coulson A & Knowles J (1970) Uniquely labelled active site sequence in chicken muscle triose phosphate isomerase. *Nature* **227**, 180–181.
- 18 Webb MR & Knowles JR (1974) The existence of an electrophilic component in the reaction catalysed by triose phosphate isomerase. *Biochem J* **141**, 589.
- 19 Belasco JG & Knowles JR (1980) Direct observation of substrate distortion by triosephosphate isomerase using Fourier transform infrared spectroscopy. *Biochemistry* **19**, 472–477.
- 20 Straus D, Raines R, Kawashima E, Knowles JR & Gilbert W (1985) Active site of triosephosphate isomerase: *in vitro* mutagenesis and characterization of an altered enzyme. *Proc Natl Acad Sci USA* **82**, 2272–2276.
- 21 Alber T, Davenport R, Giammona D, Lolis E, Petsko G & Ringe D (1987) Crystallography and site-directed mutagenesis of yeast triosephosphate isomerase: what can we learn about catalysis from a “simple” enzyme? *Cold Spring Harb Symp Quant Biol* pp. 603–613. Cold Spring Harbor Laboratory Press.
- 22 Knowles JR (1991) Enzyme catalysis: not different, just better. *Nature* **350**, 603–613.
- 23 Knowles JR (1991) To build an enzyme. *Philos Trans R Soc Lond B Biol Sci* **332**, 115–121.
- 24 Lodi PJ, Chang LC, Knowles JR & Komives EA (1994) Triosephosphate isomerase requires a positively charged active site: the role of lysine-12. *Biochemistry* **33**, 2809–2814.
- 25 Rieder SV & Rose IA (1959) The mechanism of the triosephosphate isomerase reaction. *J Biol Chem* **234**, 1007–1010.
- 26 Williams JC, Zeelen JP, Neubauer G, Vriend G, Backmann J, Michels PA, Lambeir A-M & Wierenga RK (1999) Structural and mutagenesis studies of leishmania triosephosphate isomerase: a point mutation can convert a mesophilic enzyme into a superstable enzyme without losing catalytic power. *Protein Eng* **12**, 243–250.
- 27 Borchert TV, Abagyan R, Jaenicke R & Wierenga RK (1994) Design, creation, and characterization of a stable, monomeric triosephosphate isomerase. *Proc Natl Acad Sci USA* **91**, 1515–1518.
- 28 Ray SS, Singh SK & Balaram P (2001) An electrospray ionization mass spectrometry investigation of 1-anilino-8-naphthalene-sulfonate (ANS) binding to proteins. *J Am Soc Mass Spectrom* **12**, 428–438.
- 29 Bhattacharjya S & Balaram P (1997) Hexafluoroacetone hydrate as a structure modifier in proteins: characterization of a molten globule state of hen egg-white lysozyme. *Protein Sci* **6**, 1065–1073.
- 30 Hameed M, Ahmad B, Fazili KM, Andrabi K & Khan RH (2007) Different molten globule-like folding intermediates of hen egg white lysozyme induced by high pH and tertiary butanol. *J Biochem* **141**, 573–583.
- 31 Gokhale RS, Ray SS, Balaram H & Balaram P (1999) Unfolding of Plasmodium falciparum triosephosphate isomerase in urea and guanidinium chloride: evidence for a novel disulfide exchange reaction in a covalently cross-linked mutant. *Biochemistry* **38**, 423–431.
- 32 Pray TR, Reiling KK, Demirjian BG & Craik CS (2002) Conformational change coupling the dimerization and activation of KSHV protease. *Biochemistry* **41**, 1474–1482.
- 33 Lolis E, Alber T, Davenport RC, Rose D, Hartman FC & Petsko GA (1990) Structure of yeast triosephosphate isomerase at 1.9 Å resolution. *Biochemistry* **29**, 6609–6618.
- 34 Rietveld AW & Ferreira ST (1998) Kinetics and energetics of subunit dissociation/unfolding of TIM: the importance of oligomerization for conformational persistence and chemical stability of proteins. *Biochemistry* **37**, 933–937.

- 35 Emsley P & Cowtan K (2004) Coot: model-building tools for molecular graphics. *Acta Crystallographica Section D* **60**, 2126–2132.
- 36 Emsley P, Lohkamp B, Scott WG & Cowtan K (2010) Features and development of Coot. *Acta Crystallographica Section D* **66**, 486–501.
- 37 Banerjee M, Balaram H & Balaram P (2009) Structural effects of a dimer interface mutation on catalytic activity of triosephosphate isomerase. *FEBS J* **276**, 4169–4183.
- 38 Elias M, Wieczorek G, Rosenne S & Tawfik DS (2014) The universality of enzymatic rate–temperature dependency. *Trends Biochem Sci* **39**, 1–7.
- 39 González-Mondragón E, Zubillaga RA, Saavedra E, Cháñez-Cárdenas ME, Pérez-Montfort R & Hernández-Arana A (2004) Conserved cysteine 126 in triosephosphate isomerase is required not for enzymatic activity but for proper folding and stability. *Biochemistry* **43**, 3255–3263.
- 40 Hernández-Santoyo A, Domínguez-Ramírez L, Reyes-López CA, González-Mondragón E, Hernández-Arana A & Rodríguez-Romero A (2012) Effects of a buried cysteine-to-serine mutation on yeast triosephosphate isomerase structure and stability. *Int J Mol Sci* **13**, 10010–10021.
- 41 Brown FK & Kollman PA (1987) Molecular dynamics simulations of “loop closing” in the enzyme triose phosphate isomerase. *J Mol Biol* **198**, 533–546.
- 42 Joseph D, Petsko GA & Karplus M (1990) Anatomy of a conformational change: hinged” lid” motion of the triosephosphate isomerase loop. *Science* **249**, 1425–1428.
- 43 Xiang J, Sun J & Sampson NS (2001) The importance of hinge sequence for loop function and catalytic activity in the reaction catalyzed by triosephosphate isomerase. *J Mol Biol* **307**, 1103–1112.
- 44 Casteleijn MG, Alahuhta M, Groebel K, El-Sayed I, Augustyns K, Lambeir AM, Neubauer P & Wierenga RK (2006) Functional role of the conserved active site proline of triosephosphate isomerase. *Biochemistry* **45**, 15483–15494.
- 45 Samanta M (2011) Exploring the role of highly conserved residues in triosephosphate isomerase. PhD Thesis, Indian Institute of Science, Bangalore.
- 46 Knowles JR & Jencks WP (1976) The intrinsic pK_a-values of functional groups in enzymes: improper deductions from the Ph-dependence of steady-state parameter. *Crit Rev Biochem Mol Biol* **4**, 165–173.
- 47 Lambeir AM, Backmann J, Ruiz-Sanz J, Filimonov V, Nielsen JE, Kursula I, Norledge BV & Wierenga RK (2000) The ionization of a buried glutamic acid is thermodynamically linked to the stability of *Leishmania mexicana* triose phosphate isomerase. *Eur J Biochem* **267**, 2516–2524.
- 48 Ranie J, Kumar VP & Balaram H (1993) Cloning of the triosephosphate isomerase gene of *Plasmodium falciparum* and expression in *Escherichia coli*. *Mol Biochem Parasitol* **61**, 159–169.
- 49 Anderson A & Cooper R (1970) Genetic mapping of a locus for triosephosphate isomerase on the genome of *Escherichia coli* K 12. *J Gen Microbiol* **62**, 329–334.
- 50 Shenoy AR & Visweswariah SS (2003) Site-directed mutagenesis using a single mutagenic oligonucleotide and DpnI digestion of template DNA. *Anal Biochem* **319**, 335–336.
- 51 Bradford MM (1976) A rapid and sensitive method for the quantitation of microgram quantities of protein utilizing the principle of protein-dye binding. *Anal Biochem* **72**, 248–254.
- 52 Plaut B & Knowles J (1972) pH-dependence of the triose phosphate isomerase reaction. *Biochem J* **129**, 311–320.
- 53 Horecker BL & Kornberg A (1948) The extinction coefficients of the reduced band of pyridine nucleotides. *J Biol Chem* **175**, 385–390.
- 54 Velanker SS, Ray SS, Gokhale RS, Suma S, Balaram H, Balaram P & Murthy MRN (1997) Triosephosphate isomerase from *Plasmodium falciparum*: the crystal structure provides insights into antimalarial drug design. *Structure* **5**, 751–761.
- 55 Leslie AG & Powell HR (2007) Processing diffraction data with Mosflm. In *Evolving methods for macromolecular crystallography*, pp. 41–51. Springer.
- 56 Battye TGG, Kontogiannis L, Johnson O, Powell HR & Leslie AG (2011) iMOSFLM: a new graphical interface for diffraction-image processing with MOSFLM. *Acta Crystallographica Section D* **67**, 271–281.
- 57 Evans P (2006) Scaling and assessment of data quality. *Acta Crystallographica Section D* **62**, 72–82.
- 58 Winn MD, Ballard CC, Cowtan KD, Dodson EJ, Emsley P, Evans PR, Keegan RM, Krissinel EB, Leslie AG & McCoy A (2011) Overview of the CCP4 suite and current developments. *Acta Crystallographica Section D* **67**, 235–242.
- 59 McCoy AJ, Grosse-Kunstleve RW, Adams PD, Winn MD, Storoni LC & Read RJ (2007) Phaser crystallographic software. *J Appl Crystallogr* **40**, 658–674.
- 60 Murshudov GN, Vagin AA & Dodson EJ (1997) Refinement of macromolecular structures by the maximum-likelihood method. *Acta Crystallographica Section D* **53**, 240–255.
- 61 Murshudov GN, Skubák P, Lebedev AA, Pannu NS, Steiner RA, Nicholls RA, Winn MD, Long F & Vagin AA (2011) REFMAC5 for the refinement of macromolecular crystal structures. *Acta Crystallographica Section D* **67**, 355–367.

- 62 Laskowski RA, MacArthur MW, Moss DS & Thornton JM (1993) PROCHECK: a program to check the stereochemical quality of protein structures. *J Appl Crystallogr* **26**, 283–291.
- 63 DeLano WL (2002) The PyMol Molecular Graphics System. DeLano Scientific, San Carlos, CA.

Podcast

This article is accompanied by a podcast, listen now. Or listen in iTunes.

Supporting information

Additional supporting information may be found in the online version of this article at the publisher's web site:

Table S1. List of mutagenic primers used to generate the mutants.